Biomedicine & Pharmacotherapy 167 (2023) 115593

Contents lists available at ScienceDirect

Biomedicine & Pharmacotherapy

journal homepage: www.elsevier.com/locate/biopha

Assessment of the PARP inhibitor talazoparib photosafety profile

Alejandro Mateos-Pujante [a,b,1], M. Consuelo Jiménez [a,b,*,2], Inmaculada Andreu [a,b,*,3]

[a] Departamento de Química, Universitat Politècnica de València, Camino de Vera s/n, 46022 Valencia, Spain
[b] Unidad Mixta de Investigación Universitat Politècnica de València -Instituto de Investigación Sanitaria (IIS) La Fe, Hospital Universitari i Politècnic La Fe, Avenida de Fernando Abril Martorell 106, 46026 Valencia, Spain

ARTICLE INFO

Keywords:
Comet assay
Fluorescence microscopy
Protein photooxidation
Photoproduct
Phototoxicity
Reactive oxygen species

ABSTRACT

Talazoparib (TLZ) is a poly(adenosine diphosphate [ADP]-ribose) polymerase inhibitor employed for the treatment of breast cancer. This drug displays an absorption band in the UVA region, and therefore investigation of the possible phototoxic side-effects associated to its administration results of enormous relevance. In this context, we describe here a photochemical and photobiological study to ascertain the photosafety profile of TLZ. Concerning transient species, the singlet and triplet excited states of TLZ were detected by fluorescence ($\lambda_{max\ em}$ = 440 nm) and laser flash photolysis experiments ($\lambda_{max\ abs}$ = 400 nm), respectively. Remarkably, TLZ irradiation with UVA light in aqueous solution resulted in formation of a stable photooxidated product, TLZ-P, whose absorption band is extended until the visible region. From *in vitro* experiments, phototoxicity was revealed for the parent drug by neutral red uptake (NRU) assays, with a PIF value of *ca* 7; besides, TLZ induced formation of reactive oxygen species (ROS) and produced significant damage to both proteins and DNA. By contrast, the singlet and triplet excited states of TLZ-P were not detected, and no photodamage was observed in the NRU experiments. Overall, the results indicate that TLZ induces phototoxicity, whereas its photoproduct exhibits photosafety.

1. Introduction

Poly(adenosine diphosphate [ADP]-ribose) polymerases (PARPs) are a family of enzymes involved in a variety of cellular processes, including DNA repair, transcription regulation, apoptosis, and necrosis [1–3]. Specifically, PARP1 and PARP2 are members of this family that play critical roles in the DNA single-strand breaks (SSBs) repair [4,5]. This function is inhibited by PARP inhibitors (PARPis), which have demonstrated their ability to decrease the proliferation of cancer cells, containing mutations in homologous recombination (HR) DNA repair deficiency, such as *BRCA1* or *BRCA2* genes [6,7]. In this context, PARPis provoke synthetic lethality that consist of the formation and accumulation of double-strand breaks (DSB) and, thus, cells deficient in *BRCA1/2* genes are unable to repair this DNA damage by HR, causing cellular death [8]. To understand the cytotoxic effects displayed by anticancer PARPis, this family of drugs has been investigated using multidimensional fluorescence microscopy, revealing mechanisms of sensitivity and resistance [9].

Talazoparib ((8 S,9 R)− 5-fluoro-8-(4-fluorophenyl)− 9-(1-methyl-1 H-1,2,4-triazol-5-yl)− 2,7,8,9-tetrahydro-3 H-pyrido[4,3,2 de] phthalazin-3-one, TLZ, inset in Fig. 1) is a PARPi developed by Pfizer and approved in 2018 in USA and 2019 in EU for the treatment of germline BRCA-mutated, HER2-negative breast cancer [6,10]. In this context, a randomized phase 3 trial in patients with advanced breast cancer and a germline BRCA1/2 mutation revealed a significant benefit in the treatment with TLZ over the standard chemotherapy [11]. Thus, considering patient treated-reported outcomes for TLZ that displayed a tolerable safety profile, TLZ was incorporated into the routine management of germline BRCA-mutated locally advanced/metastatic breast cancer [12]. However, according to a proteomic study, TLZ could not overcome resistance to treat triple-negative breast cancer cells [13]. In addition, TLZ is also used in patients with various solid tumors [14,15], in metastatic castration-resistant prostate cancer (mCRPC) [16] and has been considered a new candidate for the treatment of glioblastoma, since it produces radiosensitization effects in radioresistant glioblastoma cancer stem cells combined with high linear energy transfer

* Corresponding authors at: Departamento de Química, Universitat Politècnica de València, Camino de Vera s/n, 46022 Valencia, Spain.
E-mail addresses: mcjimene@qim.upv.es (M.C. Jiménez), iandreur@qim.upv.es (I. Andreu).
[1] ORCID: 0000-0003-1571-7162
[2] ORCID: 0000-0002-8057-4316
[3] ORCID: 0000-0003-3409-9443

https://doi.org/10.1016/j.biopha.2023.115593
Received 27 June 2023; Received in revised form 22 September 2023; Accepted 25 September 2023
Available online 2 October 2023

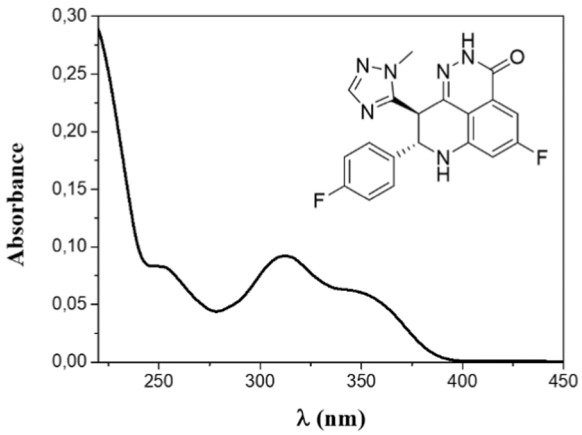

Fig. 1. Absorption spectrum of talazoparib 10 μM in PBS. Inset: chemical structure of talazoparib.

irradiation [17].

Studies regarding the nanoformulation of this drug noted that the formulation would allow for a more extended release of the drug delivered intraperitoneal to the disease site, which could offer a therapeutic advantage over the oral delivery administration [18]. In this context, from a pharmacokinetic point of view, metabolism of TLZ was negligible in humans, and renal excretion is the main route of elimination [14].

Although TLZ has a manageable tolerability profile in patients, it presents side effects, including fatigue, nausea, vomiting, diarrhea, anorexia, headache, alopecia, skin disorders, anemia, neutropenia and thrombocytopenia. The uncommon but potentially severe adverse events include myelodysplastic syndromes, marked myelosuppression and embryo-fetal toxicity [10]. In connection with adverse reactions, we have previously reported that rucaparib, another PARPi, induces cellular phototoxicity [19]. With this background, and taking into account that TLZ displays an absorption band in the UVA region, we decided to investigate its photobehavior and photobiological properties through *in vitro* studies in human skin cells (HaCaT keratinocyte cells) and proteins to advise photoprotection guidelines to patients if required and, thus, minimize the photosensitizing risk from the drug.

2. Materials and methods

2.1. Chemical and reagents

All chemicals and solvents employed were of the highest purity available from their commercial house and used without further treatments. Specifically, Talazoparib (TLZ, CAS 1207456–01–6) was purchased from TargetMol.

For cell culture experiments, human immortalized keratinocyte (HaCaT) cell line was acquired from ThermoFisher Scientific. Dulbecco's Modified Eagle Medium (DMEM), containing low glucose, L-glutamine, phenol red and penicillin-streptomycin solution (1×10^5 U/mL, 1×10^5 μg/mL) were supplied by Invitrogen. Fetal bovine serum (FBS) and trypsin-EDTA (0.25–0.02%) were acquired from Cultek. Human serum albumin fatty acid free (HSA), phosphate buffer saline (PBS) tablets and neutral red dye solution were purchased from Sigma-Aldrich.

2.2. Cell culture experiments

Human immortalized keratinocytes were cultured in plastic flasks with a surface area of 75 cm^2 and grown in DMEM supplemented with 10% FBS, 100 U/mL penicillin and 100 μg/mL streptomycin in a humidified incubator at 37% at 5% CO_2. Splitting cells were routinely done twice a week with 1:5 and 2:5 ratios and prior to each experiment, the viability of cell cultures was checked by the trypan blue exclusion assay [20].

2.3. Photophysical measurements

Absorption spectra were registered on a Jasco V-650 UV/Vis spectrophotometer in PBS at room temperature, using 1 cm quartz cuvettes.

Steady-state fluorescence measurements in PBS solution were recorded on a Jasco FP-8500 spectrofluorometer system equipped with a monochromator in the wavelength range of 200 – 850 nm at room temperature, using 1 cm quartz cuvettes, while a BioTek Synergy H1 multimode microplate reader in 96-well black plates was employed when working with cells.

Time-resolved fluorescence lifetimes (PBS, room temperature 1 cm quartz cuvettes) were measured using an EasyLife X system, which included a sample compartment with an automated peltier cuvette holder for temperature control (set to 25 °C), a pulsed LED excitation source and a lifetime detector. The wavelength of the excitation source was λ = 310 nm, and a WG370 emission filter was employed.

Phosphorescence spectra were obtained in ethanol using an Edinburg spectrofluorometer FS5 outfitted with a 150 W CW Ozone-free Xenon arc lamp and a SC-70 module with liquid nitrogen EPR Dewar. The samples were placed in 5 mm quartz tube diameter and cooled at 77 K through liquid nitrogen. The excitation wavelength was λ = 300 nm.

Laser flash photolysis (LFP) measurements were executed with a pulsed Nd YAG L52137 V LOTIS TII laser at λ_{exc} = 355 nm (Sp Lotis TII, Minsk, Belarus), where the single pulse duration was approximately 10 ns with an energy of 12 mJ per pulse. The LFP system was also equipped with a 77 250 Oriel monochromator and a Tektronix DP04054 oscilloscope. The absorbance of the samples was set to 0.30 at λ = 355 nm and solutions were deaerated by bubbling nitrogen over 15 min. Experiments were accomplished in PBS at room temperature, using 1 cm quartz cuvettes.

The triplet excited state quenching constant by oxygen (k_q) was determined employing the Stern-Volmer Eq. (1), where τ and τ_0 correspond to the triplet lifetime in the absence or presence of quencher (O_2), respectively.

$$\frac{1}{\tau} = \frac{1}{\tau_0} + k_q \cdot [O_2] \quad (1)$$

Singlet oxygen ($^1O_2$) was detected by near-infrared emission upon laser excitation at 355 nm, employing the same equipment described above with a single pulse energy of 15 mJ per pulse. The lifetime of the generated singlet oxygen was recorded at 1275 nm with a Hamamatsu NIR emission detector (peltier cooled at −62.8 °C operating at 800 V, coupled to a grating monochromator). Sample absorbance was adjusted to *ca.* 0.8 at the same wavelength and decay traces were registered in aerated conditions. The singlet oxygen quantum yield (ϕ_Δ) of TLZ was determined according to the following Eq. (2), using tetramethyl-*p*-benzoquinone (DQ) in acetonitrile as standard [21].

$$\phi_\Delta^{TLZ} = \phi_\Delta^{DQ} \cdot \frac{\Delta A_{TLZ}}{\Delta A_{DQ}} \cdot \frac{n_{DQ}}{n_{TLZ}} \quad (2)$$

Where ϕ_Δ^{DQ} corresponds to the quantum yield of the standard (0.89), [21] ΔA_{TLZ} and ΔA_{DQ} are the absorbances of TLZ and DQ, n_{DQ} and n_{TLZ} the refractive index of DQ and TLZ solvents, respectively.

2.4. Irradiation equipment

Irradiation experiments were performed in a Luzchem multi-lamp LCZ-4 photoreactor equipped with six top and eight side Hitachi lamps (λ_{max} = 350 nm, Gaussian distribution, Luzchem, Canada). Preparative irradiation was performed in a covered beaker under stirring. The course of the reaction was followed by absorption and fluorescence

spectroscopies.

For cellular culture experiments [neutral red uptake (NRU), comet, reactive oxygen species (ROS)] and protein carbonylation assays, irradiations were conducted in well-transparent plates to mitigate the effect of UVB radiation during the experiments since the plastic lid filters all radiation below 310 nm. Moreover, plates were kept on ice to avoid overheating during the experiment.

The irradiation dose was calculated using Eq. 3, where the irradiance is obtained by multiplying the powermeter detector reading by the calibration factor.

$$Irradiation\quad dose\quad \left(\frac{J}{cm^2}\right) = \frac{Irradiation\quad time(\min)\cdot Irradiance\quad \left(\frac{mW}{cm^2}\right)\cdot 60}{1000} \tag{3}$$

2.5. Steady-state irradiation and photoproduct isolation

Irradiation of TLZ (20 mg) was carried out in PBS (200 mL) at room temperature for 30 min, under stirring. The crude reaction was then lyophilized, washed with ethyl acetate (100 mL) and filtered. The solid was taken and stirred with ethyl acetate-methanol (80:20, 3 ×20 mL). After filtration, the liquid phase was evaporated *in vacuo*, to afford a magenta viscous oil. Final purification was done by high-performance liquid chromatography (HPLC, JASCO UV-1575 intelligent UV/Vis detector, JASCO PU-2080 plus intelligent HPLC Pump, JASCO LG-2080–04 quaternary gradient unit and JASCO DG-2080–54–4 line degasser) using a reverse phase column (C18 mediterranea™ sea, 25 ×1 cm), methanol-acetonitrile 50:50 v:v as mobile phase and a flow of 2 mL/min. The purification process was monitored by UV detection at 254 nm.

The isolated photoproduct (TLZ-P) was characterized by NMR spectroscopy (Bruker Advance 400 spectrometer) and high-resolution mass spectrometry using Waters ACQUITY™ XevoQToF Spectrometer (Waters Corp.) connected to the Ultra Performance Liquid Chromatography (UPLC) system, *via* an electrospray ionization interface. This source was operated in positive ionization mode at 100 °C with the capillary voltage at 1.9 kV and a desolvation temperature of 300 °C. The UPLC was carried out on a BEH C18 column (50 mm × 2.1 mm i.d., 1.7 μm) maintained at 40 °C.

5-fluoro-8-(4-fluorophenyl)− 6-hydroxy-9-(1-methyl-1 H-1,2,4-triazol-5-yl)− 2,7-dihydro-3 H-pyrido[4,3,2-de]phthalazin-3-one (TLZ-P): ^{1}H NMR (400 MHz, CD_3OD) δ 8.09 (s, 1 H), 7.70 (d, J = 11.6, 1 H), 7.47–7.43 (m, 2 H), 7.13–7.09 (m, 2 H), 3.64 (s, 3 H); ^{13}C NMR (100 MHz, CD_3OD) 180.3, 178.5, 167.1, 165.6, 163.2, 159.5, 152.4, 151.6, 150,6, 138.8, 136.3, 133.2, 132.5, 119.4, 118.1, 117.9, 116.2, 115.3, 98.1, 36.5, 24.2. HRMS (ESI-TOF): *m/z* calculated for $C_{19}H_{13}F_2N_6O_2$ [MH^+] 395.1068, found [MH^+] 395.1064. See Fig. S1 in Online Resource for further details.

2.6. Neutral red uptake (NRU) assay

The phototoxicity test was executed in accordance with the OECD guideline 432 [22] with minor modifications: the assays were performed employing human immortalized keratinocytes (HaCaT) rather than BALB/c 3T3 fibroblasts since their similarity with human skin cells has already been reported [23], and irradiations were performed in free phenol red DMEM to avoid UV absorption by phenol red. In brief, cells were seeded in two 96-well plates for each compound at a density of 2×10^4 cells/well. The next day, the culture media was replaced with free phenol red DMEM and cells were subsequently treated with TLZ or TLZ-P at eight different concentrations ranging from 2.5 to 500 μM, where SDS and CPZ were used as negative and positive controls, respectively. After 1 h of incubation, one plate was exposed to a 5 J/cm^2 UVA radiation dose (according to the mentioned OECD guideline 432) under the described conditions, while the other was kept in the dark. All compound solutions were immediately replaced with DMEM medium and plates were incubated overnight. The next day, 20 μL of a neutral red solution (50 μL/mL) was added to all wells and plates were incubated for 2 h at 37 ºC. Then, cells were washed once with PBS and neutral red was extracted from lysosomes by adding 100 μL of a fresh extraction buffer (50% Milli-Q water, 49.5% ethanol, 0.5% acetic, v-v). Absorbance values were registered at 550 nm on a Synergy H1 microplate reader and, for each compound, dose-response curves were plotted by non-linear regression to obtain the IC_{50} values (compound concentration resulting in a 50% reduction in the neutral red uptake) in dark and UVA light conditions with GraphPad Prism 5.03 software. Finally, the photoirritation factor (PIF) values were calculated using the next Eq. (4).

$$PIF = \frac{IC_{50}(dark)}{IC_{50}\quad (UVA)light} \tag{4}$$

In accordance with the OECD Guideline, a compound is predicted as phototoxic if PIF is higher than 5, probably phototoxic if PIF lies between 2 and 5, and non-phototoxic if PIF is lower than 2.

Additionally, given that TLZ-P absorbs light in the visible region, another NRU experiment was carried out employing 14 LZC-LGR visible light lamps (λ_{max} = 520 nm, Gaussian distribution, Luzchem, Canada), to check if the photoproduct was able to induce phototoxicity under these conditions. For this purpose, rose bengal (RB) was used as the positive control [24] instead of CPZ, whereas SDS was maintained as the negative control.

2.7. Reactive oxygen species (ROS) detection

To evaluate oxidative-stress induced phototoxicity, the quantity of ROS produced by TLZ after UVA radiation was measured using 2′,7′-dichlorodihydrofluorescein diacetate (H_2DCF-DA), a profluorescent probe that, after penetrating cell membrane, is deacetylated by intracellular esterases to produce 2′,7′-dichlorodihydrofluorescein (H_2DCF). H_2DCF fluoresces when it is oxidized by ROS to yield 2′,7′-dichlorofluorescein (DCF) [25].

Keratinocytes were seeded into two 12-well plates (4×10^4 cells/well). After 24 h, the culture media was replaced with free phenol red DMEM containing TLZ (85 or 100 μM) or RCP 10 μM (employed as the positive control [19]) and incubated for 1 h. Then, one plate was irradiated at a 5 J/cm^2 UVA dose, while the other was kept in the darkness. Afterward, compounds were removed by replacing the media with a H_2DCF-DA solution (25 μM) in PBS and incubated for 30 min in dark. Finally, cells were washed twice with PBS and fluorescence images were retrieved using a Leica DMI 4000B fluorescence microscopy (λ_{exc} = 495 nm, λ_{em} = 525 nm) employing the Fluorescein FITC filter. Representative images were selected from two different wells in different regions of each condition.

2.8. Photoinduced protein oxidation assay

Detection of protein carbonyl formation photoinduced by TLZ was assessed by means of 2,4-dinitrophenylhydrazine (DNPH) derivatization assay [26] with slight modifications, using human serum albumin (HSA) as a protein model. Summarily, HSA solutions (5 mg/mL) in PBS were prepared, incubated with increasing concentrations of TLZ (65, 75, 85 μM) at room temperature for 1 h and irradiated with increasing concentrations of a UVA dose (0, 5, 10, 15 J/cm^2). Immediately after, samples were treated with DNPH (200 μL, 10 mM) and incubated in darkness at room temperature for 1 h to allow the formation of dinitrophenyl hydrazone adducts. Proteins were subsequently precipitated by adding trichloroacetic acid (TCA, 1 mL, 20% v/v), incubated on ice for 15 min and centrifuged at 13,000 rpm for 5 min. Then, after discarding the supernatants, pellets were washed twice by adding a solution of ethanol/ethyl acetate (1 mL, 50:50, v/v), containing 20% TCA to remove the unbound DNPH, and dried at 60 ºC for 15 min to fully evaporate the solvent. Finally, adducts were then solved in guanidine

hydrochloride (100 μL, 6 M) overnight at 4 ºC and absorbance at 375 nm was recorded using the Synergy H1 microplate reader. The degree of HSA oxidation was expressed as nmol of carbonyl content per mg protein according to the Eq. (5):

$$Carbonyl\quad content\quad (nmol/mg\quad protein) = \frac{(A_{sample} - A_{blank})\cdot 100}{6.364} \qquad (5)$$

Where the value of 6.364 corresponds to ε at 375 nm x l (the length of the path light for a 96-well plate).

2.9. Alkaline comet assay

The well-known single-cell electrophoresis assay (comet assay) was carried out as previously described, [27] with minor modifications. Cells were harvested, resuspended in PBS and placed on ice for 2 h to allow keratinocytes to repair mild DNA damage induced by trypsin detachment. Subsequently, cells were seeded in two 24-well plates (5×10^4 cells/well), treated with TLZ (85 μM) or the positive control (CPZ, 5 μM) and incubated at 4 ºC for 30 min in darkness. Then, one plate was exposed to a 5 J/cm^2 UVA radiation dose, while the other was kept in dark conditions as negative control. After mixing 100 μL of each suspension with 100 μL of 1% low melting point agarose solution, droplets were poured into Trevigen treated slides and placed on an ice-cold tray to allow them to gel. The slides were then submerged inside coupling jars filled with a lysis buffer [19] and finally they were maintained at 4 ºC overnight to permit cell lysis.

The following day, the electrophoresis was set up at ≈ 300 mA (corresponding to 21 V) over 30 min at 4 ºC in a Trevigen comet assay electrophoresis tank, loaded with all slides and coated with 1 L of alkaline electrophoresis buffer cooled [19]. At the end of electrophoresis, slides were washed twice with distilled water for 5 min. DNA was fixed by two subsequent incubations in 70% and 100% ethanol solutions over 5 min each and dried in a heater at 37 ºC for 2 h. Afterward, DNA nucleoids and tails were stained with SYBR Gold [1:10,000 dilution in TE buffer (10 mM Tris-HCl pH 7.5, 1 mM EDTA)] for 30 min at 4 ºC in darkness, washed once with Milli-Q water, air-dried and kept in darkness until further visualization. Finally, DNA nucleoids and tails were visualized using a Leica DMI 4000B fluorescence microscope (λ_{exc} = 490 nm), picking five pictures per condition. The percentage of DNA damage in each sample was determined by visual scoring of at least 100 DNA comets, utilizing the ImageJ 1.52 software and total DNA damage was established with the classification of six DNA categories [28] according to Eq. (6).

$$DNA\quad damage\quad (\%) = \frac{\sum_{n=0}^{6} n\quad class\quad comet\quad x\quad n}{6} \qquad (6)$$

To investigate if cells were able to repair DNA damage generated by TLZ upon UVA radiation, a set of recovery experiments were performed. Thus, prior to the cellular lysis, slides were maintained in non-supplemented DMEM medium at 37 ºC for 6 h and then lysed as stated above. For this purpose, 5-hydroxydiclofenac (5-OH DCF, 100 μM) was used as recovery positive control [29].

2.10. Data analysis and statistics

Results obtained are presented as mean ± standard deviation (SD) from at least three independent experiments. Chemical structures were drawn with the ChemDraw software (version 18.1). Spectroscopy measurements were plotted using the OriginPro software (version 9.0). Regression methods were developed using the GraphPad software (version 5.0). Visual scoring of comet assay experiments was analyzed by the ImageJ software (version 1.52). RMN experiments were represented and analyzed by the MestReNova software (version 6.0.2). Statistical significance was assessed by the Student's t-test, considering only p values lower than 0.05 as significant result (* $p < 0.05$, ** $p < 0.01$, *** $p < 0.001$).

3. Results and discussion

3.1. Irradiation of TLZ in aqueous medium

The UV-Vis absorption spectrum of TLZ (Fig. 1) shows that the drug absorbs light in the UVA region (315–400 nm). Since 95% of UVA sunlight is not filtered by ozone layer and reaches the Earth's surface, investigation of the UVA-induced reactivity of TLZ is a relevant issue in connection with possible drug-mediated phototoxic side-effects. After sunlight absorption, photogenerated transient species derived from TLZ could be reactive towards cell or biomolecules causing damage and/or evolving to photoproducts formation, which potential phototoxicity also would deserve to be tested.

Before addressing the biological assays, the photoreactivity of the drug was investigated in aqueous media at the same pH as the biological environment. Thus, a TLZ 20 μM PBS solution was irradiated in a photoreactor with lamps centered at λ = 350 nm. The process was monitored by following the changes in the absorption (Fig. 2a) and fluorescence spectra (Fig. 2b) at increasing irradiation times.

In the absorption measurements, the TLZ spectrum before irradiation (black trace) exhibited two maxima at λ = 310 and λ = 350 nm that disappeared after 40 min of irradiation, concomitant with the appearance of a new band with maxima at λ = 540 nm, extended until 610 nm (red trace). This feature was detectable at naked eye (Fig. 2a inset), as a change from non-colored (non-irradiated solution) to pink (after 40 min irradiation) suggesting transformation of TLZ in new photoproduct(s). Substantial changes were also observed in the fluorescence spectra, where the initial band of TLZ, centered at λ = 440 nm, decreased with increasing irradiation times (gray traces), until became almost negligible after 40 min irradiation time (red trace).

To isolate and characterize the possible photoproduct(s), a preparative irradiation was performed: thus, 20 mg of TLZ were suspended in 200 mL of PBS and irradiated for 30 min in a photoreactor at λ_{max} = 350 nm, under stirring. After liquid-liquid extraction with ethyl acetate-methanol (80:20) and evaporation of the solvent (see Materials and methods section for further details), the resulting crude was purified by HPLC (1:1 MeOH/MeCN as eluent), affording only one photoproduct (TLZ-P). The HRMS spectrum obtained by EI gave a MH^+ peak at 395.1064 uma, corresponding to M = $C_{19}H_{12}F_2N_6O_2$. This 14 uma increment respect to parent TLZ (MH^+ = 381.1191, M = $C_{19}H_{14}F_2N_6O$), matches with loss of 2 hydrogens and addition of 1 oxygen.

To ascertain TLZ-P structure, ^{1}H NMR experiments in CD_3OD were performed. Thus, a comparison between TLZ-P and TLZ spectra (Figs. S1a and S2, respectively) showed the following key features: i) the signals corresponding to H_a and H_b at δ = 4.90 ppm and δ = 5.02 ppm in TLZ are not present in the TLZ-P spectra, which is consistent with the formation of a double bond between C_a and C_b; ii) the two doublet of doublets of H_c and H_d in TLZ (δ = 6.95 and δ = 7.25 ppm) disappear in TLZ-P spectrum; instead, only one doublet at δ = 7.70 ppm is observed. This is in agreement with the presence of a hydroxyl at C_c or C_d. From the couplings observed in bidimensional HSQC and HMBC experiments (Fig. S1d and S1e), the proposed chemical structure of TLZ-P is that shown in Chart 1.

Bearing in mind that TLZ-P is a stable TLZ photoderivative that extends the absorption band to the visible region (see Fig. S3, for a comparison between TLZ and TLZ-P absorption spectra), an investigation of TLZ-P potential involvement in phototoxic issues is necessary in the context of photodamage produced by the parent drug.

3.2. Photophysical measurements

Normalized absorption and fluorescence spectra (λ_{exc} = 305 nm) of TLZ in PBS are presented in Fig. S4. The energy of the first singlet excited state (E_S), obtained from the intersection between both spectra, was

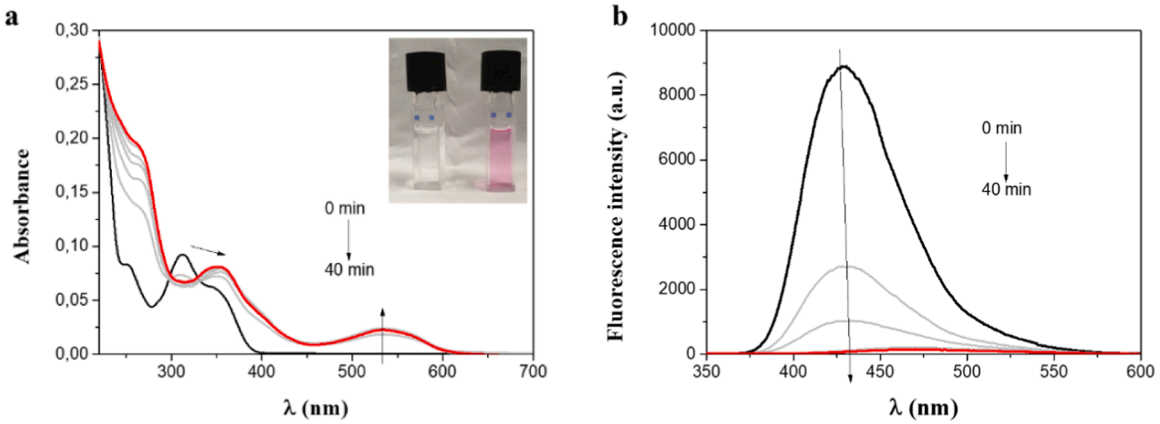

Fig. 2. Changes in the TLZ spectra (20 μM in PBS) after irradiation at λ_{exc} = 350 nm, from 0 min (black) to 40 min (red). **a**: Absorption spectra. **b**: Fluorescence spectra (λ_{exc} = 305 nm). Inset: TLZ/PBS solution after 0 min (left) and 40 min (right) irradiation.

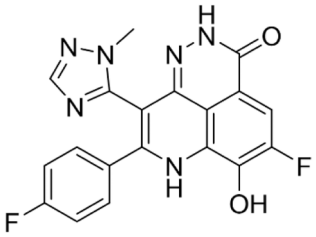

Chart 1. Chemical structure of talazoparib photoproduct, TLZ-P.

found to be 309,3 kJ mol^{-1}. The TLZ fluorescence quantum yield (ϕ_F), was 0.12 in PBS and 0.10 in cells culture [30].

The normalized TLZ phosphorescence spectrum, performed at 77 K in ethanol matrix, consisted in a band with λ_{max} = 512 nm (Fig. S4). From the 30% of the rise of the band, the first triplet excited state energy (E_T) was determined as 255,8 kJ mol^{-1} [31]. The transient absorption spectrum of TLZ (55 μM in PBS, λ_{exc} = 355 nm, N_2) was obtained by laser flash photolysis. The band, with maximum at λ = 400 nm (Fig. 3) was ascribed to the triplet excited state, based on the observed quenching by oxygen, characteristic of these species (Fig. 3 inset). The triplet lifetime (τ_T) value in N_2 atmosphere was τ_T = 8.8 μs. Experiments performed under oxygen, air and N_2 allowed to obtain the oxygen quenching constant, k_{Tq} (O_2) = 3.6 × 10^9 $M^{-1}s^{-1}$. As this species was efficiently quenched by oxygen, exploring the generation of singlet oxygen ($^1O_2$ or $^1\Delta g$) proved interesting since it can promote oxidative damage to biomolecules inside cells. Thus, for this purpose, time-resolved near-infrared emission studies upon 355 nm excitation of TLZ were performed. Formation of singlet oxygen was detected by measurements of the luminescence at 1275 nm in MeCN (Fig. 3b). To determine the singlet oxygen quantum yield (ϕ_Δ), tetramethyl-p-benzoquinone in MeCN was employed as reference (ϕ_Δ *ca.* 0.89 in MeCN) [21] and the lifetime obtained was 38 μs. As expected, TLZ can generate $^1O_2$ with a ϕ_Δ = 0.54, and therefore, the Type II mechanism is involved in the photosensitized oxidation of the target biomolecules of the cells.

The main photophysical properties of TLZ are summarized in Table 1. Unlike the parent drug, TLZ-P did not exhibit any fluorescence (Fig. S5) and no signals were detected in the LFP experiments. This suggests that the photoproduct could exhibit a photosafety profile. To investigate this hypothesis, *in vitro* neutral red uptake assay was also performed with the photoproduct.

3.3. *In vitro phototoxicity assessments*

3.3.1. *Neutral red uptake (NRU) assay*

First, the TLZ and TLZ-P photoirritant factor (PIF) values were calculated from cell viability assays (through neutral red stain) of human keratinocytes (HaCaT) cells treated with increasing amounts of

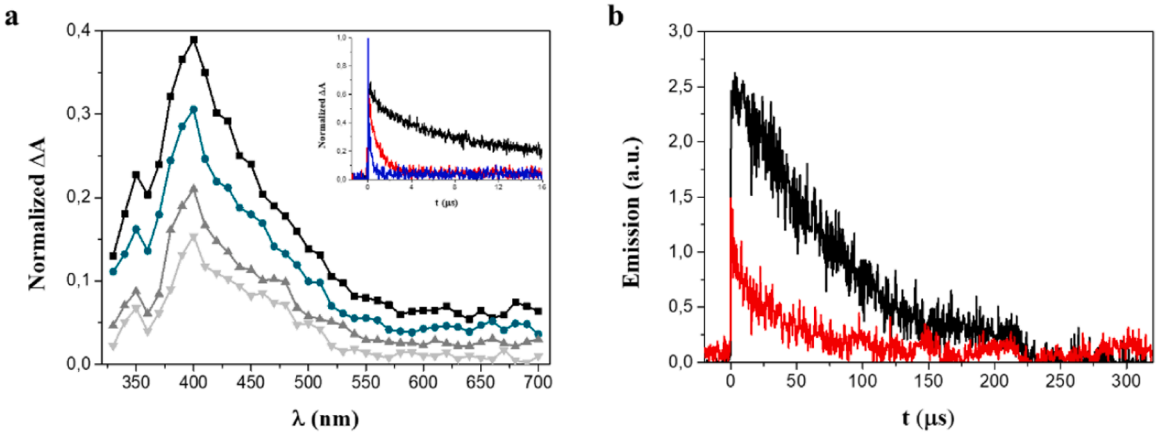

Fig. 3. **a**: Laser flash photolysis of a 55 μM TLZ solution in PBS at λ = 355 nm. Transient absorption spectra at different time windows, under N_2 atmosphere: 0.5 μs (black), 2 μs (dark cyan), 8 μs (grey) and 12 μs (fine grey). Inset: Decays monitored at λ = 400 nm under nitrogen (black), air (red) and oxygen (blue) atmospheres. **b**: Kinetic traces for $^1O_2$ signals at 1275 nm after laser pulse (λ_{exc} = 355 nm) for TLZ in MeCN (red). Tetramethyl-*p*-benzoquinone (DQ) in MeCN (black) was used as reference.

Table 1
Main photophysical properties of TLZ.

$\lambda_{max\ abs}$ (nm)[a]	250, 320, 350
$\lambda_{max\ em}$ (nm)[b]	440
E_s (kJ mol^{-1})	309.3
ϕ_F[b]	0.12
τ_F (ns)[b]	< 1 ns
$\lambda_{max\ em}$ (nm)[c]	512
E_T (kJ mol^{-1})[c]	255,8
$\lambda_{max\ abs}$ (nm)[d]	400
τ_T (μs)[d]	8.8
k_{Tq} (O_2) ($M^{-1}s^{-1}$)[d,e]	3.6×10^9
ϕ_Δ[h]	0.54
τ_Δ (μs)[h]	38

[a] Absorption spectroscopy, 20 μM, PBS, rt, air;
[b] fluorescence spectroscopy, λ_{exc} = 305 nm, 20 μM, PBS, rt, air;
[c] phosphorescence spectroscopy, λ_{exc} = 300 nm, 50 μM, ethanol, 77 K, air;
[d] transient absorption spectroscopy, λ_{exc} = 355 nm, 55 μM, PBS, rt, N_2;
[e] using Eq. 1;
[h] detected by emission at 1275 nm, 180 μM, MeCN, rt, air.

drug or photoproduct, under dark or UVA light conditions (λ_{exc} = 350 nm, light dose = 5 J/cm^2). The PIF values of well-known positive (chlorpromazine, CPZ) and negative (sodium dodecyl sulfate, SDS) controls were also determined under the same conditions, to ensure the reliability of the results. According to the OECD 432 guideline (2019), a PIF lower than 2 means "no-phototoxicity", a PIF between 2 and 5 indicates "probable phototoxicity" and PIF higher to 5 is associated to "phototoxicity". See Materials and methods section for further experimental details.

From the corresponding dose-response curves (Fig. S6) for TLZ and TLZ-P at λ_{exc} = 350 nm, their IC_{50} values were determined. Results obtained for CPZ and SDS are presented in the same Fig. S6. The TLZ PIF value was found to be 7, with IC_{50} dark > 500 μM and IC_{50} UVA light = 76 ± 14 μM. According to the above-mentioned OECD 432 guideline (2019) [22], the drug can be considered responsible to induce phototoxicity. However, for TLZ-P, both IC_{50} dark and IC_{50} UVA light resulted to be higher than 500 μM, with a PIF value of *ca.* 1. Since TLZ-P absorbs also light from the visible region (until 600 nm, see Fig. S3), its NRU assay was also performed at λ_{exc} = 520 nm, using RB as positive control instead of CPZ that does not absorb at this wavelength. From the corresponding dose-response curves (Fig. S7) a PIF value of 1 was again obtained, indicating no phototoxicity. Table 2.

These results indicates that, although the parent drug is phototoxic under UVA radiation, its phototransformation leads to a derivative non-reactive towards UVA light. Moreover, from the experiments at λ = 520 nm, it can be concluded that TLZ-P is not phototoxic either in the visible range. Hence, from now on, *in vitro* experiments were performed only for TLZ.

Table 2
TLZ and TLZ-P *in vitro* HaCaT NRU phototoxicity assay.

Compound	IC_{50} (dark)	IC_{50} (light)	PIF
CPZ	94 ± 30	4 ± 1[a]	24[c]
SDS	168 ± 46	192 ± 53[a]	1[c]
TLZ	> 500	76 ± 14[a]	7[c]
TLZ-P	> 500	> 500[a]	1[c]
RB	8 ± 3	0.4 ± 0.1[b]	20
SDS	150 ± 65	138 ± 50[b]	1
TLZ-P	> 500	> 500[b]	1

Data correspond to the mean ± SD from four experiments performed in triplicate.
[a] λ_{exc} = 350 nm;
[b] λ_{exc} = 520 nm;
[c] In agreement with the OECD 432 guideline [22], PIF lower than 2 means "no phototoxicity", PIF between 2 and 5 means "probably phototoxicity" and PIF higher than 5 means "phototoxicity".

Since reactive oxygen species (ROS) formation is frequently at the origin of biomolecules and/or cell-membranes oxidation, next step was investigation of the possible TLZ-induced ROS generation under UVA irradiation.

3.3.2. Reactive oxygen species generation

For this purpose, HaCaT cells were seeded on 12-well plates and incubated in the presence of TLZ different concentrations (0, 85 and 100 μM) or with RCP 10 μM, as positive control, either in the dark or under UVA irradiation (light dose = 5 J/cm^2). Then, cells staining was performed using 25 μM 2′,7′-dichlorodihydrofluorescein diacetate (H_2DCF-DA) and the emission of DCF was recorded by fluorescence microscopy, using a Fluorescein FITC filter. In Fig. 4, images A, C and E correspond to non-irradiated samples and images B, D and F are obtained after irradiation.

In the presence of TLZ (C) the fluorescence was almost negligible and similar to that recorded in the absence of drug (A), indicating no ROS formation. This is in agreement with the TLZ IC_{50} value obtained in the dark (> 500 μM.). By contrast, irradiated cells/TLZ mixtures exhibited fluorescence (D), pointing the ability of TLZ to generate ROS upon UVA radiation. The effect was dependent on drug concentration. As expected, the control experiment consisting in irradiation of cells in the absence of drug (B) did not gave any positive result. More details are available in Fig. S8.

Next experiments were devoted to ascertain whether the TLZ observed phototoxicity could be attributed to proteins and/or genomic DNA.

3.3.3. Protein photooxidation evaluation

Given that TLZ binds efficiently to plasma proteins and that the most frequent (usually irreversible) oxidative modification to proteins is produced by carbonylation, the carbonyl content for TLZ/human serum albumin (HSA) systems was determined, as possible early biomarker of oxidative damage. Thus, PBS solutions containing HSA (0.075 μM) and TLZ (65, 75 or 85 μM in PBS) were irradiated with different UVA light doses (0, 5, 10 and 15 J/cm^2) and the carbonyl content measured using the 2,4-dinitrophenylhydrazine (DNPH) derivatization method.

Fig. 5 shows that the carbonyl content of TLZ/HSA systems increased significantly after UVA irradiation, which clearly evidences that TLZ induces photooxidation of cellular membranes. These results are in agreement with those initially obtained upon the NRU test. Another set of experiments with higher TLZ concentration (80, 120, 160 μM) is available in the Fig. S9.

3.3.4. Photogenotoxicity by comet assay

To investigate the possibility of single-strand breaks (SSB), double-strand breaks (DSB) and alkali-labile sites formation on DNA of an individual cell [32], the comet assay under alkaline conditions was employed. To this end, HaCaT cells were incubated with TLZ 85 μM for 30 min and irradiated with UVA light for 16 min (5 J/cm^2). The resulting photolysate was embedded in agarose on a slide and alkaline electrophoresis was performed. This allowed migrating damaged and fragmented DNA away from the nucleus. After staining with SYBR Gold, the fluorescence of the comet nucleoids and tails was analyzed by fluorescence microscopy, using the Fluorescein FITC filter. The DNA damage obtained was calculated by means of visual scoring of at least 100 DNA comets. Since cell death can promote in some extent DNA fragmentation by activation of caspase activated DNases (CADs), cell viability was also assessed by trypan blue exclusion assay [20], in order to avoid misleading results. Thus, viability rate was higher than 85%, indicating the suitability of both UVA dose and drug concentration employed [33,34]. A set of experiments was also performed using HaCaT cells in the absence of TLZ (negative control) or in the presence of 5-OH DCF 100 μM (recovery positive control).

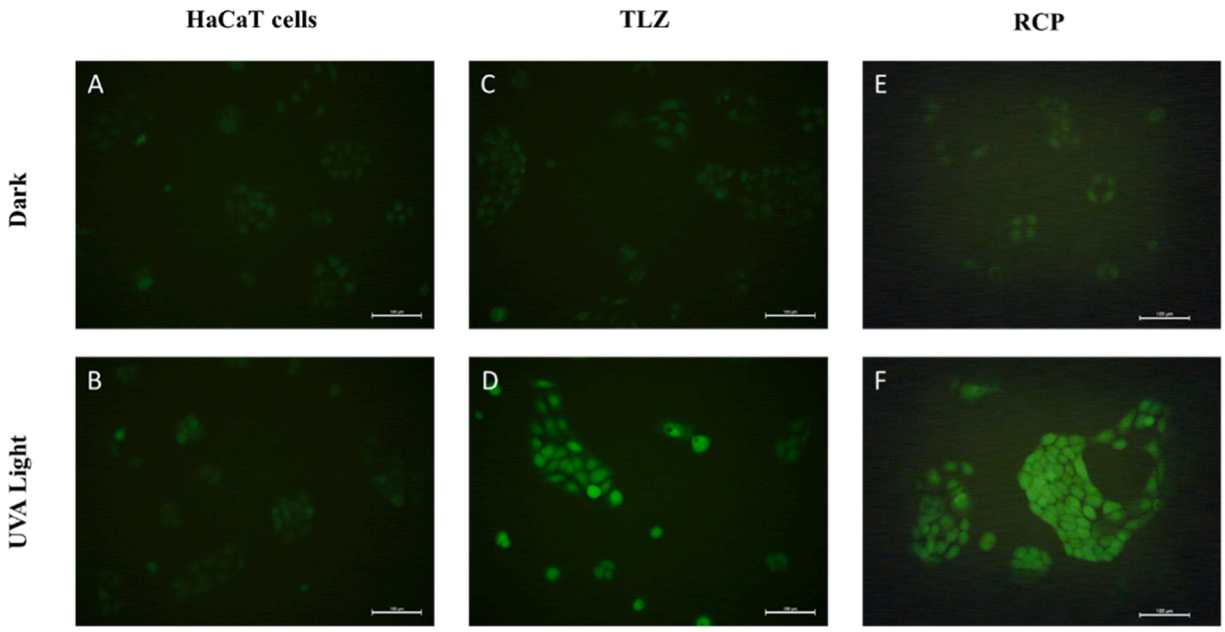

Fig. 4. ROS experiments for TLZ (100 μM): Representative photographs by fluorescence microscopy, using Fluorescein FITC as a filter. Human keratinocytes (HaCaT) cells were incubated alone (A, B), in the presence of TLZ (C, D) or RCP (E, F), maintained in the dark (A, C, E) or irradiated (B, D, F) with UVA light (5 J/cm^2). All samples were treated with 25 μM 2′,7′-dichlorodihydrofluorescein diacetate (H_2DCF-DA).

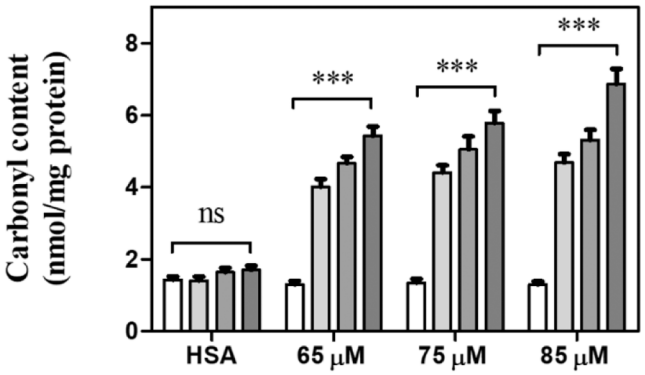

Fig. 5. Protein photooxidation by TLZ. The carbonyl content was determined using the DNPH derivatization method. Conditions: HSA: 0.075 μM; TLZ: 65, 75 or 85 μM, irradiation doses (green scale): 0 (□), 5 (▫), 10 (▪) or 15 (■) J/cm^2. Data represent mean ± SD of three independent experiments performed in triplicate Asterisks indicate significant differences by Student's t-test (ns: non-significant, *** $p < 0.001$).

Comet results are shown in Fig. 6 and Fig. S10. They were performed on HaCaT cell alone (A, D, G), in the presence of 5-OH DCF (B, E, H) or TLZ (C, F, I); A, B, C correspond to non-irradiated samples, while D, E and F are obtained after irradiation and G, H, I are after irradiation and cell recovery. No differences were observed among the non-irradiated samples (A, B, C) indicating no damage, while TLZ in combination with UVA light (F) promotes significant damage to cells (*ca.* 55%, Fig. S11), as seen when comparing with the negative (D) and positive (E) controls. It is noteworthy that, in comparison with the recovery positive control (H), no substantial reduction in nuclear DNA damage was noticed after 6 h of time recovery (I), indicating irreversible DNA damage.

Overall, the results obtained in the present work have proven that the anticancer drug talazoparib can trigger photosensitivity reactions, resulting in both phototoxic and photogenotixic to cells, as revealed in the *in vitro* experiments. From a clinical point of view, it results very interesting in identifying the cutaneous adverse events associated with targeted therapies.

4. Conclusions

Steady-state irradiations, photophysical experiments, and *in vitro* cellular and protein assays have been performed on the anticancer drug talazoparib (TLZ) to reveal if it is a photosafety drug. After UVA irradiation, TLZ photooxidizes to TLZ-P, a photoproduct that extends its absorption band to the visible region. The TLZ singlet and triplet excited states have been detected, while such transient species have not been observed for the photoproduct. This could be related with a higher phototoxicity of the parent drug than the photoproduct. In fact, from neutral red uptake assays the TLZ PIF value was 7 at $\lambda_{exc} = 350$ nm, indicating phototoxicity, whereas PIF = 1 for TLZ-P when irradiating both at UVA and visible light. Besides, reactive oxygen species generation for TLZ/keratinocytes/UVA combination has been evidenced by recording the fluorescence of 2′,7′-dichlorofluorescein, and photooxidation of protein cellular membranes has been demonstrated by measuring the increase of carbonyl content of TLZ/HSA systems after UVA irradiation. Moreover, time-resolved near-infrared emission studies reveal the formation from the triplet excited state of singlet oxygen, which can promote photodamage to biomolecules inside cells. Finally, irreversible DNA damage was found in the comet assays, indicating that TLZ could also be considered a photogenotoxic drug. The collective results indicate unambiguously that TLZ exhibits phototoxicity after UVA irradiation, which is relevant to advise photoprotection guidelines to patients with cancer and, thus, minimize the photosensitizing risk from the drug.

Funding information

Grants: PID2020-115010RB-I00 and PID2022-1381890NB-I00 funded by MICIN/AEI/10.13039/501100011033 and by "ERDF A way of making Europe" , CIAICO/2021/061 and ACIF/2018/153 fellowship for A. M.-P funded by Generalitat Valenciana.

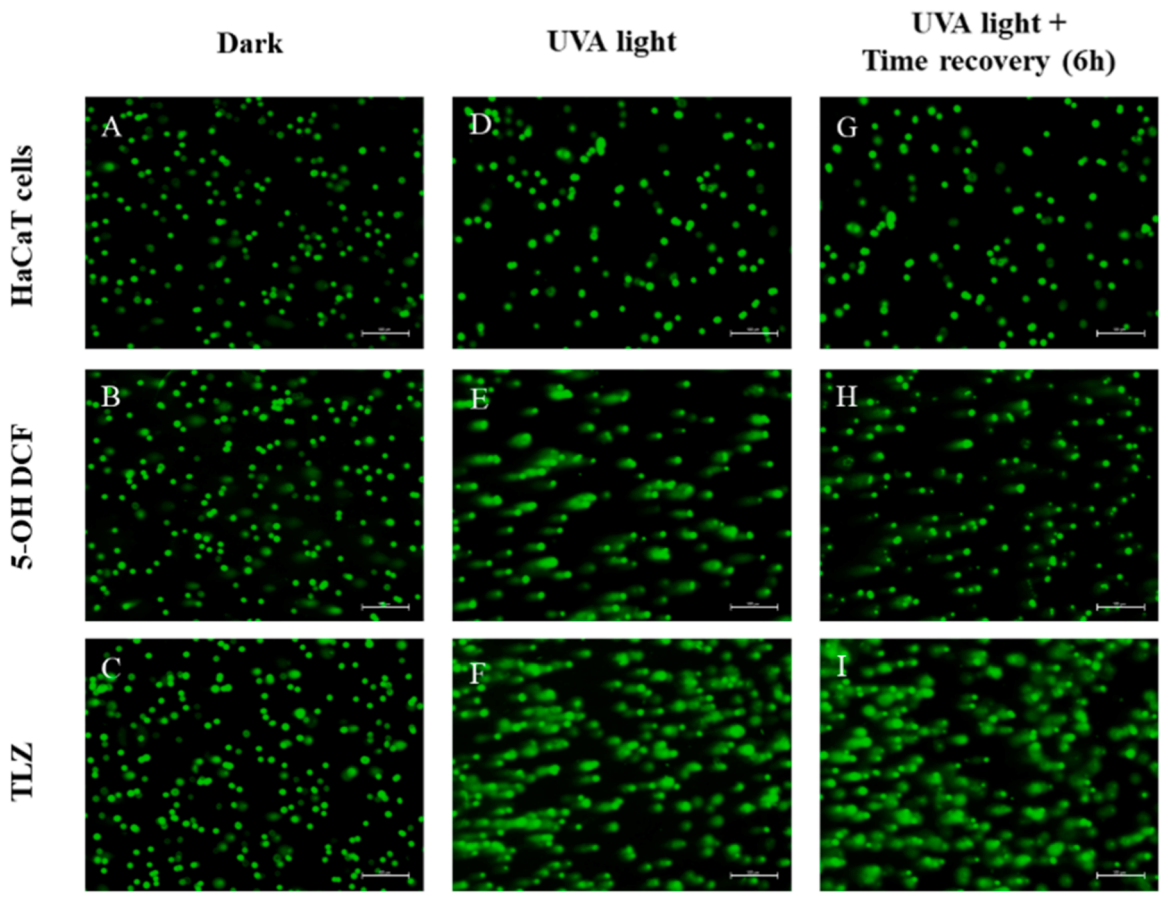

Fig. 6. Representative fluorescence microscopy images (fluorescein FITC filter) of comet assay experiments. Human keratinocytes (HaCaT) cells were incubated alone (A, D, G), in the presence of 5-OH DCF (B, E, H) and TLZ (C, F, I) in the dark (A, B, C), upon UVA irradiation (D, E, F) or upon UVA irradiation followed by 6 h recovery (G, H, I).

CRediT authorship contribution statement

Alejandro Mateos-Pujante: Experimental work: photophysical measurements, in vitro experiments, preparative irradiations, spectroscopic characterization, Writing-editing. **M. Consuelo Jiménez:** Conceptualization, Methodology, Formal analysis, Writing – original draft, Writing – review & editing. **Inmaculada Andreu:** Conceptualization, Methodology, Formal analysis, Writing – original draft, Writing – review & editing.

Declaration of Competing Interest

The authors declare the following financial interests/personal relationships which may be considered as potential competing interests: Inmaculada Andreu reports financial support was provided by State Agency of Research. M. Consuelo Jimenez reports financial support was provided by Conselleria de innovación, universidades, ciencia y sociedad digital. Alejandro Mateos-Pujante reports financial support was provided by Conselleria de innovación, universidades, ciencia y sociedad digital.

Data Availability

Data will be made available on request.

Appendix A. Supporting information

Supplementary data associated with this article can be found in the online version at doi:10.1016/j.biopha.2023.115593.

References

[1] Z. Herceg, Z.-Q. Wang, Functions of poly(ADP-ribose) polymerase (PARP) in DNA repair, genomic integrity and cell death, Mutat. Res. 477 (2001) 97–110, https://doi.org/10.1016/S0027-5107(01)00111-7.
[2] S. Vyas, M. Chesarone-Cataldo, T. Todorova, Y.H. Huang, P. Chang, A systematic analysis of the PARP protein family identifies new functions critical for cell physiology, Nat. Commun. 4 (2013), 2240, https://doi.org/10.1038/ncomms3240.
[3] M.-F. Langelier, T. Eisemann, A.A. Riccio, J.M. Pascal, PARP family enzymes: regulation and catalysis of the poly(ADP-ribose) posttranslational modification, Curr. Opin. Struct. Biol. 53 (2018) 187–198, https://doi.org/10.1016/j.sbi.2018.11.002.
[4] A. Ray Chaudhuri, A. Nussenzweig, The multifaceted roles of PARP1 in DNA repair and chromatin remodelling, Nat. Rev. Mol. Cell Biol. 18 (2017) 610–621, https://doi.org/10.1038/nrm.2017.53.
[5] J. Ménissier de Murcia, M. Ricoul, L. Tartier, C. Niedergang, A. Huber, F. Dantzer, V. Schreiber, J.C. Amé, A. Dierich, M. LeMeur, L. Sabatier, P. Chambon, G. de Murcia, Functional interaction between PARP-1 and PARP-2 in chromosome stability and embryonic development in mouse, EMBO J. 22 (2003) 2255–2263, https://doi.org/10.1093/emboj/cdg206.
[6] B. Wang, D. Chu, Y. Feng, Y. Shen, M. Aoyagi-Scharber, L.E. Post, Discovery and Characterization of (8S,9R)-5-Fluoro-8-(4-fluorophenyl)-9-(1-methyl-1H-1,2,4-triazol-5-yl)-2,7,8,9-tetrahydro-3H-pyrido[4,3,2-de]phthalazin-3-one (BMN 673, Talazoparib), a Novel, Highly Potent, and Orally Efficacious Poly(ADP-ribose) Polymerase-1/2 Inhibitor, as an Anticancer Agent, J. Med. Chem. 59 (2016) 335–357, https://doi.org/10.1021/acs.jmedchem.5b01498.
[7] L. Cortesi, H.S. Rugo, C. Jackisch, An overview of PARP inhibitors for the treatment of breast cancer, Target. Oncol. 16 (2021) 255–282, https://doi.org/10.1007/s11523-021-00796-4.
[8] C.J. Lord, A. Ashworth, PARP inhibitors: Synthetic lethality in the clinic, Science 355 (2017) 1152–1158, https://doi.org/10.1126/science.aam7344.
[9] J. Michelena, A. Lezaja, F. Teloni, T. Schmid, R. Imhof, M. Altmeyer, Analysis of PARP inhibitor toxicity by multidimensional fluorescence microscopy reveals mechanisms of sensitivity and resistance, Nat. Commun. 9 (2018), 2678, https://doi.org/10.1038/s41467-018-05031-9.
[10] S.M. Hoy, Talazoparib: first global approval, Drugs 78 (2018) 1939–1946, https://doi.org/10.1007/s40265-018-1026-z.

[11] J.K. Litton, H.S. Rugo, J. Ettl, S.A. Hurvitz, A. Gonçalves, K.-H. Lee, L. Fehrenbacher, R. Yerushalmi, L.A. Mina, M. Martin, H. Roché, Y.-H. Im, R.G. W. Quek, D. Markova, I.C. Tudor, A.L. Hannah, W. Eiermann, J.L. Blum, Talazoparib in patients with advanced breast cancer and a germline BRCA mutation, N. Engl. J. Med. 379 (2018) 753–763, https://doi.org/10.1056/NEJMoa1802905.

[12] S.A. Hurvitz, A. Gonçalves, H.S. Rugo, K.H. Lee, L. Fehrenbacher, L.A. Mina, S. Diab, J.L. Blum, J. Chakrabarti, M. Elmeliegy, L. DeAnnuntis, E. Gauthier, A. Czibere, I.C. Tudor, R.G.W. Quek, J.K. Litton, J. Ettl, Talazoparib in patients with a germline BRCA-mutated advanced breast cancer: detailed safety analyses from the phase III EMBRACA trial, Oncologist 25 (2020) e439–e450, https://doi.org/10.1634/theoncologist.2019-0493.

[13] G. Guney Eskiler, S. Yanar, G. Akpinar, M. Kasap, Proteomic analysis of talazoparib resistance in triple-negative breast cancer cells, J. Biochem. Mol. Toxicol. 35 (2021), e22678, https://doi.org/10.1002/jbt.22678.

[14] Y. Yu, C.H. Chung, A. Plotka, K. Quinn, H. Shi, Z. Pápai, L. Nguyen, D. Wang, A phase 1 mass balance study of (14) C-labeled talazoparib in patients with advanced solid tumors, J. Clin. Pharmacol. 59 (2019) 1195–1203, https://doi.org/10.1002/jcph.1415.

[15] S. Boussios, C. Abson, M. Moschetta, E. Rassy, A. Karathanasi, T. Bhat, F. Ghumman, M. Sheriff, N. Pavlidis, Poly (ADP-Ribose) polymerase inhibitors: talazoparib in ovarian cancer and beyond, Drugs R. D. 20 (2020) 55–73, https://doi.org/10.1007/s40268-020-00301-8.

[16] J.S. de Bono, N. Mehra, G.V. Scagliotti, E. Castro, T. Dorff, A. Stirling, A. Stenzl, M. T. Fleming, C.S. Higano, F. Saad, C. Buttigliero, I.M. van Oort, A.D. Laird, M. Mata, H.C. Chen, C.G. Healy, A. Czibere, K. Fizazi, Talazoparib monotherapy in metastatic castration-resistant prostate cancer with DNA repair alterations (TALAPRO-1): an open-label, phase 2 trial, Lancet Oncol. 22 (2021) 1250–1264, https://doi.org/10.1016/s1470-2045(21)00376-4.

[17] P. Lesueur, F. Chevalier, E.A. El-Habr, M.P. Junier, H. Chneiweiss, L. Castera, E. Müller, D. Stefan, Y. Saintigny, Radiosensitization effect of talazoparib, a parp inhibitor, on glioblastoma stem cells exposed to low and high linear energy transfer radiation, Sci. Rep. 8 (2018), 3664, https://doi.org/10.1038/s41598-018-22022-4.

[18] P. Baldwin, A.W. Ohman, J.E. Medina, E.T. McCarthy, D.M. Dinulescu, S. Sridhar, Nanoformulation of talazoparib delays tumor progression and ascites formation in a late stage cancer model, Front. Oncol. 9 (2019), 353, https://doi.org/10.3389/fonc.2019.00353.

[19] A. Mateos-Pujante, M.C. Jiménez, I. Andreu, Evaluation of phototoxicity induced by the anticancer drug rucaparib, Sci. Rep. 12 (2022), 3434, https://doi.org/10.1038/s41598-022-07319-9.

[20] W. Strober, Trypan Blue Exclusion Test of Cell Viability, A3.B.1-a3.B.3, Curr. Protoc. Immunol. 111 (2015), https://doi.org/10.1002/0471142735.ima03bs111.

[21] I. Gutiérrez, S.G. Bertolotti, M.A. Biasutti, A.T. Soltermann, N.A. García, Quinones and hydroxyquinones as generators and quenchers of singlet molecular oxygen, Can. J. Chem. 75 (1997) 423–428, https://doi.org/10.1038/s41598-022-07319-9.

[22] OECD, Test No. 432: In Vitro 3T3 NRU Phototoxicity Test, OECD Guidelines for the Testing of Chemicals, Section 4, (2019). https://doi.org/10.1787/9789264071162-en.

[23] A.R. Svobodová, J. Ultichová, J. Vostálová, Human keratinocyte cell line as a suitable model for in vitro phototoxicity testing, . Bras. Dermatol. 94 (2019) 105–106, https://doi.org/10.1590/abd1806-4841.20197620.

[24] A.K. Srivastav, S.F. Mujtaba, A. Dwivedi, S.K. Amar, S. Goyal, A. Verma, H. N. Kushwaha, R.K. Chaturvedi, R.S. Ray, Photosensitized rose Bengal-induced phototoxicity on human melanoma cell line under natural sunlight exposure, J. Photochem. Photobiol. B, Biol. 156 (2016) 87–99, https://doi.org/10.1016/j.jphotobiol.2015.12.001.

[25] X. Wang, M.G. Roper, Measurement of DCF fluorescence as a measure of reactive oxygen species in murine islets of Langerhans, Anal. Methods 6 (2014) 3019–3024, https://doi.org/10.1039/c4ay00288a.

[26] G. Colombo, M. Clerici, M.E. Garavaglia, D. Giustarini, R. Rossi, A. Milzani, I. Dalle-Donne, A step-by-step protocol for assaying protein carbonylation in biological samples, J. Chromatogr. B. 1019 (2016) 178–190, https://doi.org/10.1016/j.jchromb.2015.11.052.

[27] F. Palumbo, G. Garcia-Lainez, D. Limones-Herrero, M.D. Coloma, J. Escobar, M. C. Jiménez, M.A. Miranda, I. Andreu, Enhanced photo(geno)toxicity of demethylated chlorpromazine metabolites, Toxicol. Appl. Pharmacol. 313 (2016) 131–137, https://doi.org/10.1016/j.taap.2016.10.024.

[28] P. Møller, Assessment of reference values for DNA damage detected by the comet assay in human blood cell DNA, Mutat. Res. 612 (2006) 84–104, https://doi.org/10.1016/S0027-5107(01)00111-7.

[29] G. Garcia-Lainez, A.M. Martínez-Reig, D. Limones-Herrero, M. Consuelo Jiménez, M.A. Miranda, I. Andreu, Photo(geno)toxicity changes associated with hydroxylation of the aromatic chromophores during diclofenac metabolism, Toxicol. Appl. Pharmacol. 341 (2018) 51–55, https://doi.org/10.1016/j.taap.2018.01.005.

[30] W.H. Melhuish, Quantum efficiences of fluorescence of organic substances: effect of solvent and concentration of the fluorescent solute, J. Phys. Chem. 65 (1961) 229–235, https://doi.org/10.1021/j100820a009.

[31] A.C. Marco Montalti, Luca Prodi, M. Teresa Gandolfi, Handbook of Photochemistry, CRC Press, Boca Raton, 2006.

[32] A.R. Collins, The comet assay. Principles, applications, and limitations, Methods Mol. Biol. 203 (2002) 163–177, https://doi.org/10.1385/1-59259-179-5:163.

[33] A. Azqueta, A.R. Collins, The essential comet assay: a comprehensive guide to measuring DNA damage and repair, Arch. Toxicol. 87 (2013) 949–968, https://doi.org/10.1007/s00204-013-1070-0.

[34] M. Glei, T. Schneider, W. Schlörmann, Comet assay: an essential tool in toxicological research, Arch. Toxicol. 90 (2016) 2315–2336, https://doi.org/10.1007/s00204-016-1767-y.